Dramatic Switching of Magnetic Exchange in a Classic Transition Metal Oxide: Evidence for Orbital Ordering

Wei Bao,[1,2] C. Broholm,[1,3] G. Aeppli,[4] P. Dai,[5] J. M. Honig,[6] and P. Metcalf[6]
[1]*Department of Physics and Astronomy, The Johns Hopkins University, Baltimore, Maryland 21218*
[2]*Physics Department, Brookhaven National Laboratory, Upton, New York 11973*
[3]*National Institute of Standards and Technology, Gaithersburg, Maryland 20899*
[4]*NEC, 4 Independence Way, Princeton, New Jersey 08540*
[5]*Solid State Division, Oak Ridge National Laboratory, Oak Ridge, Tennessee 37831*
[6]*Purdue University, West Lafayette, Indiana 47907*
(Received 26 August 1996)

Spin correlations in metallic and insulating phases of V_2O_3 and its derivatives are investigated using magnetic neutron scattering. Metallic samples have incommensurate spin correlations varying little with hole doping. Paramagnetic insulating samples have spin correlations only among near neighbors. The transition from either of these phases into the low temperature insulating antiferromagnetic phase is accompanied by an abrupt change of dynamic magnetic short range order. Our results support the idea that the transition into the antiferromagnetic insulator is also an orbital ordering transition. [S0031-9007(96)02178-3]

PACS numbers: 71.27.+a, 71.30.+h, 75.30.Et, 75.40.Gb

Orbital order and disorder have been popular ingredients for explanations of many curious phenomena in solids, most notably the transition metal oxides [1,2]. In spite of large interest among condensed matter physicists, the evidence for nontrivial, in the sense of not simply being due to conventional spin-orbit coupling, orbital fluctuations and order is generally quite indirect. We have been able to make progress by taking advantage of a very sensitive measure of electronic orbitals, namely the exchange interactions linking the spins on neighboring atoms, which are determined by integrals over outer electron wave functions. In particular, we report the discovery of a dramatic switching of magnetic exchange interactions on moving between the high and low temperature insulating phases of the classic transition metal oxide V_2O_3. The switching is most naturally explained in terms of an orbital ordering transition. In addition, we find that the high temperature spin fluctuations in metallic V_2O_3 are insensitive to hole doping, showing little evolution on going from a stoichiometric sample with an insulating antiferromagnetic ground state to a sample which remains metallic down to the lowest temperatures and displays a low moment spin density wave (SDW). Furthermore, the magnetic fluctuations in the paramagnetic metal are similar to those in the paramagnetic insulator, which suggest that orbital fluctuations play an important role in the metal as well as in the insulator.

Figure 1 shows the phase diagram of V_2O_3 as a function of temperature and two kinds of doping. Vanadium deficiency drives the material metallic by populating the $3d$ band with holes, while Cr^{3+} ($3d^3$) substitution for V^{3+} ($3d^2$) stabilizes an insulating state [3]. Three single crystal samples studied in this work, and indicated by color bars on the figure, cover all four phases of V_2O_3. The samples were grown using a skull melter and in the stoichiometric and vanadium deficient samples, oxygen content was controlled to within $\delta y = 0.003$ by annealing sliced crystals for two weeks at 1400 °C in a suitably chosen CO-CO_2 atmosphere [4]. The sensitivity of our experiment was increased by mutually aligning several crystals so that the total mass reached ~15 g for $V_{1.973}O_3$, 8 g for V_2O_3 (Néel temperature $T_N = 170$ K) and 6.4 g in the case of $(V_{0.97}Cr_{0.03})_2O_3$ ($T_N = 180$ K).

The neutron scattering experiments were carried out on thermal neutron triple axis spectrometers at NIST and

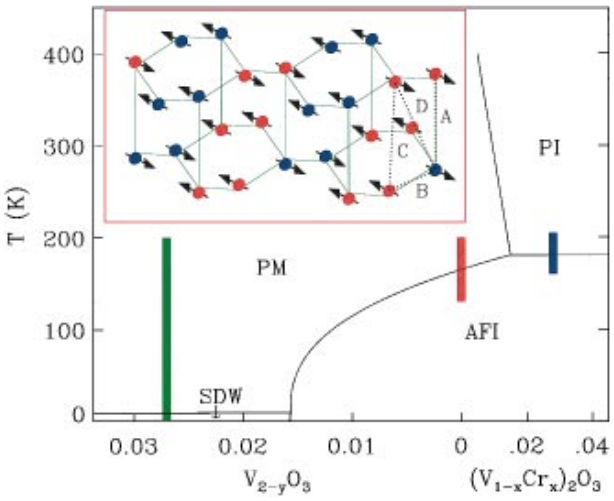

FIG. 1(color). Phase diagram of V_2O_3 [3]. PI denotes the paramagnetic insulating phase; PM, the paramagnetic metallic phase; AFI, the antiferromagnetic insulating phase; and SDW, the metallic spin-density-wave phase. The PM-PI phase boundary terminates at a critical point. The color bars mark the samples and the temperature ranges explored in this work. Inset: spin and orbital orders in the AFI phase [2,5]. The two degenerate (in the single ion limit) vanadium orbitals are represented by red and blue, respectively. *A-D* label four kinds of near-neighbor pairs.

ORNL. A graphite filter was used to remove high-order neutrons. After correcting for the $\hbar\omega$-dependent efficiency of the spectrometer, the magnetic neutron scattering intensity was normalized to inelastic scattering from transverse acoustic phonons to yield absolute measurements of the dynamic spin correlation function,

$$S(\mathbf{Q},\omega) = \frac{1}{2}\sum_{\alpha\beta}(\delta_{\alpha\beta} - \hat{Q}_\alpha\hat{Q}_\beta)|F(Q)|^2\frac{(g\mu_B)^2}{2\pi N\hbar} \times \int dt\; e^{i\omega t}\sum_{\mathbf{R}\mathbf{R}'} e^{-i\mathbf{Q}\cdot(\mathbf{R}-\mathbf{R}')}\langle S^\alpha_{\mathbf{R}}(t)S^\beta_{\mathbf{R}'}(0)\rangle. \quad (1)$$

Wave vector $\mathbf{Q}$ will be indexed in the hexagonal reciprocal lattice with $a^* = 4\pi/\sqrt{3}a = 1.47(1)$ Å^{-1} and $c^* = 2\pi/c = 0.448(1)$ Å^{-1} in the metallic phases, $a^* = 1.46(1)$ Å^{-1} and $c^* = 0.449(2)$ Å^{-1} in the AFI phase, and $a^* = 1.45(1)$ Å^{-1} and $c^* = 0.451(2)$ Å^{-1} in the PI phase.

We begin by surveying the spin fluctuations in three of the phases of V_2O_3: the metallic antiferromagnet (SDW), the metallic paramagnet (PM), and the insulating paramagnet (PI) (Fig. 1). Other workers have successfully surveyed spin waves in the fourth phase, the insulating antiferromagnet (AFI) [6]. Figures 2(a) and 2(b) show contour maps of the dynamic spin correlation function $S(\mathbf{Q},\omega)$ in metallic antiferromagnetic $V_{1.973}O_3$ at 1.4 K and in paramagnetic, but still metallic V_2O_3 at 200 K. In both cases we observe ridges, with bandwidths exceeding 18 meV and centered near $\mathbf{Q} = (1,0,\overline{0.3})$ and (1,0,2.3), wave vectors which characterize the magnetic order in the hole-doped material (e.g., $V_{1.973}O_3$) [7]. As is appropriate, given the higher temperature for frame (b) than frame (a), the ridges are sharper for frame (a). On moving to the PI phase [Fig. 2(c)] at nearly the same temperature, however, there is further broadening. Indeed, the data are now best described as a single broad ridge along the $\hbar\omega$ axis centered at $\mathbf{Q} = (1,0,0.8)$. From the half-width-at-half-maximum of constant energy cuts through this ridge [see Fig. 3(d) and Ref. [8]], we estimate spin correlation lengths $\xi_c \approx 1.5$ Å and $\xi_a \approx 2.0$ Å along the c axis and in the basal plane, respectively.

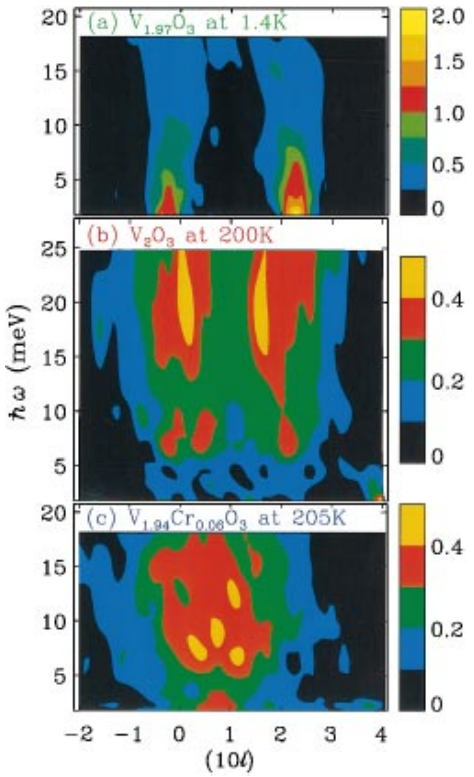

FIG. 2(color). Contour maps of $S(\mathbf{Q},\omega)$ for $\mathbf{Q}$ along the (10ℓ) direction in (a) $V_{1.973}O_3$ at 1.4 K, (b) V_2O_3 at 200 K, and (c) $(V_{0.97}Cr_{0.03})_2O_3$ at 205 K. Intensity is indicated by the color bars in units of μ_B^2/meV per unit cell, which contains 6 formula units. The $\mathbf{Q}$ range covers a Brillouin zone, with nuclear Bragg points (102) and (104) at the ends. Resolutions in both $\mathbf{Q}$ and ω are narrower than the widths of features by at least a factor 2 [9,8] [see, e.g., Figs. 3(b) and 3(d)].

One of the most remarkable features of the metal-insulator transition in V_2O_3 is that the antiferromagnetic order (see inset of Fig. 1) which develops in the insulator is different from the SDW which occurs in vanadium deficient samples [7,9]. Specifically, as may also be seen in the inset of Fig. 1, vanadium atoms in V_2O_3 have three nearest neighbors within a puckered honeycomb plane. In the SDW phase each spin is approximately antiparallel to all of its three in-plane neighbors, whereas in the AFI the threefold symmetry is broken with one nearest neighbor parallel, the two others antiparallel. The two types of local spin arrangements are conveniently labeled (10ℓ)-type and $(0.5,0.5,\ell)$-type, respectively, according to which line in reciprocal space contains the magnetic Bragg peaks of the corresponding long range ordered structure. In the following we show that irrespective of whether we consider static or dynamic properties, $(0.5,0.5,\ell)$-type

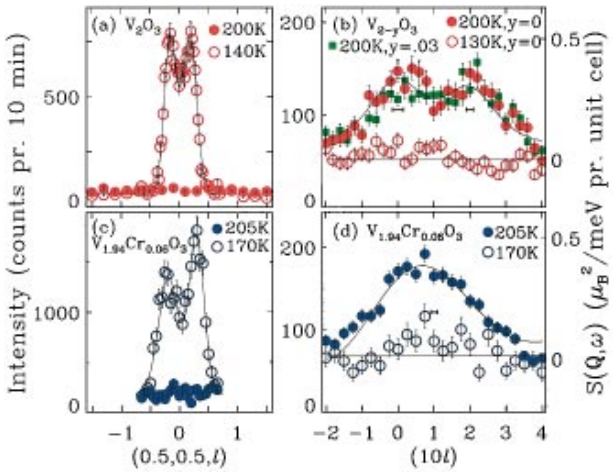

FIG. 3(color). Constant $\hbar\omega = 9$ meV scans along (10ℓ) and constant $\hbar\omega = 12$ meV scans along $(0.5,0.5,\ell)$ for $V_{2-y}O_3$ [(a) and (b)] and $(V_{0.97}Cr_{0.03})_2O_3$ [(c) and (d)] inside (open symbols) and outside (filled symbols) the AFI phase. (10ℓ) scans look similar over explored $\hbar\omega$ range (see Fig. 2). The horizontal bars indicate the FWHM of the projection of the resolution function on the scan direction. Peaks in (a) and (c) are resolution limited. We use $E_f = 13.7$ meV. Collimations are 60′-40′-40′-80′, 60′-40′-80′-80′, and 60′-40′-40′-60′ at NIST for (a), (b), and (d), respectively; (c) shows data from ORNL with 50′-40′-40′-70′.

correlations exist only in the AFI phase while $(1, 0, \ell)$-type correlations exist only outside this phase.

To probe dynamic correlations corresponding to the two structures, we performed constant-energy scans along each of these two directions in reciprocal space. The results are shown in Fig. 3 where the right and left columns probe (10ℓ)-type and $(0.5, 0.5, \ell)$-type correlations, respectively. Filled symbols correspond to high temperature phases and open symbols to the AFI. For both $V_{2-y}O_3$ (top frames) and $V_{1.94}Cr_{0.06}O_3$ (bottom frames), (10ℓ)-type correlations are visible only outside the AFI phase, whereas $(0.5, 0.5, \ell)$-type correlations can be seen only in the AFI phase. Entry to the AFI phase not only changes the near-neighbor correlations, it also brings about coherence in the magnetic excitations as evidenced by the resolution-limited double peaks in Figs. 3(a) and 3(c). These correspond to the excitation of counter-propagating spin waves in the long range ordered antiferromagnet [6]. Such dramatic modifications of spin dynamics indicate that exchange interactions undergo profound changes at the transition to the AFI. Meanwhile, doping to produce either an insulating phase by Cr substitution or a more metallic sample by decreasing the V to O ratio has a much smaller effect on the spin dynamics at fixed temperature within the paramagnetic phase. Indeed, Fig. 3(b) shows that at 200 K, the magnetic fluctuations in V_2O_3 and $V_{1.97}O_3$, which have AFI and metallic SDW ground states, respectively, are identical.

Figure 4 gives the detailed temperature dependence of dynamic spin correlations for V_2O_3 and $V_{1.94}Cr_{0.06}O_3$.

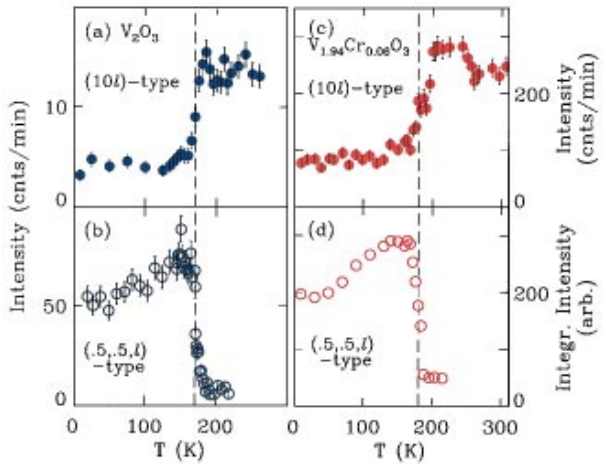

FIG. 4(color). Temperature variations of the neutron scattering intensity from (10ℓ)-type and $(0.5, 0.5, \ell)$-type magnetic fluctuations in pure V_2O_3 [(a) and (b)] and $(V_{0.97}Cr_{0.03})_2O_3$ [(c) and (d)]. (10ℓ)-type fluctuations at $\hbar\omega = 9$ meV were probed with $\mathbf{Q} = (1, 0, 2)$ in (a) and $\mathbf{Q} = (1, 0, 0, 8)$ in (c). $(0.5, 0.5, \ell)$-type fluctuations at $\hbar\omega = 12$ meV were monitored at $\mathbf{Q} = (0.5, 0.5, 0.2)$ in (b), while we report the $(0.5, 0.5, \ell)$ $\mathbf{Q}$-integrated intensity in (d). The dashed lines indicate the location of the phase transition out of the AFI as determined by the disappearance of a magnetic Bragg peak at $\mathbf{Q} = (0.5, 0.5, 0)$. All data were acquired upon increasing temperature from $T = 1.4$ K.

Coincident with the transition to the AFI phase (vertical dashed lines) is an abrupt switch between the two types of dynamic spin correlations. A remarkable similarity exists between the transitions to the AFI phase from the paramagnetic metal (V_2O_3, left column) and from the paramagnetic insulator ($V_{1.94}Cr_{0.06}O_3$, right column), which suggests a common mechanism which is independent of whether or not a Fermi surface, associated with metallic behavior, exists in the high temperature phase.

Our discoveries find no comprehensive explanation within a one-band Hubbard model [10]. The most serious difficulty is the abrupt switch of the magnetic wave vector which occurs at the transition to the AFI. In addition the insulating paramagnet is characterized by magnetic correlations which are shorter ranged than those of the paramagnetic metal. Like many single-band Hubbard calculations, the doped copper oxides which eventually become high temperature superconductors display none of these anomalous features.

The most obvious potential cause for the anomalous short range correlations in the PI phase is that conventional exchange interactions between spins lead to a frustrated Heisenberg model which is unable to develop long range order at $T \sim J/k_B$. Solid state chemistry, however, speaks against this possibility because only A and B types of nearest neighbors (see Fig. 1) have appreciable exchange interactions in V_2O_3 [2] and a Heisenberg model with only these interactions is not frustrated [11].

A more likely explanation of our data is based on work of Castellani *et al.* who established how covalent bonding between doubly degenerate $3d$ orbitals control the sign and magnitude of spin-spin interactions in V_2O_3 [2]. The basic idea is that the magnetically active electron on a single vanadium ion can exist in one of two degenerate orbitals. Even so, the exchange integrals, which determine the coupling between spins on neighboring ions, depend strongly on which orbitals are occupied. Indeed, when orbitals on neighboring ions are orthogonal, the resulting spin coupling is ferromagnetic, while if they are not, the coupling tends to be antiferromagnetic. The net Hamiltonian for insulating V_2O_3 then involves orbital as well as spin degrees of freedom at each site, where the spin-orbit coupling is not a bilinear coupling on a single site, as in conventional magnets, but actually involves the relative spin and orbital occupancies on neighboring sites [2]. Castellani *et al.* examined many possible orbital configurations for V_2O_3 and concluded that the most likely is that represented by the colors used to locate the V ions in Fig. 1. Here the magnetic unit cell is doubled in the basal planes because the orbital ordering doubles the unit cell also. On warming through T_N, we are left with disorder in both spin and orbital occupancies. The magnetic short range order in the paramagnetic phase then depends on whether we are looking at frequencies (a) large or (b) small compared to the relaxation rate Γ_{orb} characterizing the orbital fluctuations. When (a) $\omega \gg \Gamma_{\text{orb}}$, the interactions with the neighbors will be similar to those below

T_N, and we expect to see heavily damped renditions of the spin waves seen below T_N. On the other hand, if (b) $\omega \ll \Gamma_{\rm orb}$, one can average over the orbital degrees of freedom and obtain an effective spin Hamiltonian where all couplings are antiferromagnetic.

We now consider whether limit (a) or (b) is more appropriate for our $(V_{0.97}Cr_{0.03})_2O_3$ sample. Obviously, because we see no remnants of the low-temperature spin waves, description (a) cannot apply. We can check whether (b) applies, especially in the detailed sense of its prediction that all interactions are antiferromagnetic, by rewriting the observed structure factor $S(\mathbf{Q}, \omega)$ as the Fourier transform of the two-spin correlation function in real space and then checking the signs of the near-neighbor correlations. A remarkably good fit ($\chi^2 = 1.5$) to the experimental $S(\mathbf{Q}, \omega)$ [12] is obtained when we truncate the series to include correlations among only four types of spin pairs (see inset of Fig. 1). More specifically, we find that $\langle \mathbf{S}_0 \cdot \mathbf{S}_{[0,0,1/6+\delta]} \rangle^A = 0.6(3)$, $\langle \mathbf{S}_0 \cdot \mathbf{S}_{[1/3,2/3,\bar{\delta}]} \rangle^B = -0.19(8)$, $\langle \mathbf{S}_0 \cdot \mathbf{S}_{[2/3,1/3,\delta-1/6]} \rangle^C = 0.18(8)$, and $\langle \mathbf{S}_0 \cdot \mathbf{S}_{[2/3,1/3,1/6]} \rangle^D = -0.09(3)$, where $\delta = 0.026$ and we normalized so that $\langle \mathbf{S}_0 \cdot \mathbf{S}_0 \rangle = 1$. The curve through the 205 K data in Fig. 3(d) was calculated using this model. Thus measurable correlations are not all antiferromagnetic and we do not have a state (b) with complete orbital disorder, i.e., with $\Gamma_{\rm orb}/\omega \to \infty$. Simultaneously, though, the antiferromagnetic correlations are very short ranged in spite of the fact that the temperature and measuring frequencies are below the exchange constants characterizing the AFI phase [6]. The most probable cause is that while $k_B T$ and $\hbar\omega$ are somewhat lower than $\Gamma_{\rm orb}$, they are close enough to $\Gamma_{\rm orb}$ that the spin couplings, fluctuating with the orbital occupancies, have effectively random signs which give rise to magnetic frustration. In other words, we are proposing that the orbital fluctuation rate is of order $k_B T \approx 20$ meV.

Finally, what happens in the metallic state? Here we can no longer speak about local orbital and spin degrees of freedom, but it is still possible to make Wannier projections of analogous objects from the band states. Our finding that the magnetic correlations in the metallic state are much more similar to those in the PI than in the AFI corroborates the assignment by Takigawa *et al.* [13] of the nuclear magnetic relaxation primarily to orbital rather than spin fluctuations in metallic V_2O_3. Even so, the orbital fluctuations may be somewhat faster than in the PI because the antiferromagnetic correlations are further ranged (i.e., there are resolvably sharper peaks in $S(\mathbf{Q}, \omega)$ for the PM phase) and the PM-AFI transition appears more strongly first order than the PI-AFI transition [6].

To summarize, we have discovered that the magnetic fluctuations in V_2O_3 switch dramatically as a function of temperature as the antiferromagnetic insulating state is entered from either insulating or metallic paramagnetic phases. They change in a much more modest fashion as a function of doping and temperature in the paramagnetic phase, be it metallic or insulating. We conclude that the primary order parameter for the AFI phase is orbital, and that orbital order drives the spin ordering not via a conventional spin-orbit interaction for each V ion, but instead via a long-range ordered modulation of the exchange constants coupling spins on different V ions. The orbital ordering breaks translational symmetry and is the orbital analog of antiferromagnetism. This is to be contrasted with the celebrated orbital order in the cubic uranium pnictides [14], which while it leads to spectacular anisotropies, does not break translation symmetry and indeed can be traced to single-ion spin-orbit coupling. Finally, our data represent strong evidence for the long-standing notion that orbital, charge, and spin degrees of freedom need to be considered on an equal footing near the metal-insulator transition in generic transition metal oxides.

We gratefully acknowledge discussions with S. K. Sinha, T. M. Rice, G. Kotliar, Q. M. Si, G. Sawatzky, L. F. Mattheiss, and R. J. Birgeneau. W. B. thanks the Aspen Center for Physics where part of the work was performed. Work at JHU was supported by the NSF through DM-9453362, at ORNL by DOE under Contract No. DE-AC05-84OR21400, at BNL by DOE under Contract No. DE-AC02-76CH00016, and J. M. H. was supported on MISCON Grant No. DE-FG02-90ER45427.

[1] K. I. Kugel and D. I. Khomskii, Sov. Phys.—JETP **37**, 725 (1973); H. F. Pen *et al.* (to be published).
[2] T. M. Rice, in *Spectroscopy of Mott Insulators and Correlated Metals*, edited by A. Fujimori and Y. Tokura (Springer, New York, 1995); C. Castellani, C. R. Natoli, and J. Ranninger, Phys. Rev. B **18**, 4945 (1978); **18**, 4967 (1978); **18**, 5001 (1978).
[3] D. B. McWhan *et al.*, Phys. Rev. Lett. **27**, 941 (1971); Y. Ueda *et al.*, Mater. Res. Bull. **12**, 87 (1977).
[4] S. A. Shivashankar *et al.*, J. Electrochem. Soc. **128**, 2472 (1981); **129**, 1641 (1982).
[5] R. M. Moon, Phys. Rev. Lett. **25**, 527 (1970).
[6] R. E. Word *et al.*, Phys. Rev. B **23**, 3533 (1981); M. Yethiraj *et al.*, *ibid.* **36**, 8675 (1987).
[7] W. Bao *et al.*, Phys. Rev. Lett. **71**, 766 (1993).
[8] W. Bao *et al.* (to be published).
[9] W. Bao *et al.*, Phys. Rev. B **54**, 3726R (1996).
[10] T. Moriya and H. Hasegawa, J. Phys. Soc. Jpn. **48**, 1490 (1980); M. Cyrot and P. Lacour-Gayet, Solid State Commun. **11**, 1767 (1972); X. Y. Zhang *et al.*, Phys. Rev. Lett. **70**, 1666 (1993); M. J. Rozenberg *et al.*, Phys. Rev. B **49**, 10 181 (1994); T. Pruschke *et al.*, *ibid.* **47**, 3553 (1993); A. Georges and W. Krauth, *ibid.* **48**, 7167 (1993).
[11] F. Bertaut, Comput. Rend. Acad. Sci. **252**, 252 (1961); N. Menyuk and K. Dwight J. Phys. Chem. Solids **25**, 1031 (1964).
[12] C. Broholm *et al.*, J. Appl. Phys. **79**, 5023 (1996). Included in the fits were scans from (1,0,$\bar{10}$) to (1,0,10), from (001) to (201), and from (005) to (205).
[13] M. Takigawa *et al.*, Phys. Rev. Lett. **76**, 283 (1996).
[14] G. H. Lander *et al.*, Phys. Rev. Lett. **40**, 523 (1978); S. K. Sinha *et al.*, *ibid.* **45**, 1028 (1980); Phys. Rev. B **23**, 4556 (1981).